Applied Catalysis B: Environmental 150–151 (2014) 230–237

Contents lists available at ScienceDirect

Applied Catalysis B: Environmental

journal homepage: www.elsevier.com/locate/apcatb

Review

$PdTe_x$/C nanocatalysts with high catalytic activity for ethanol electro-oxidation in alkaline medium

Jindi Cai, Yiyin Huang, Yonglang Guo*

College of Chemistry and Chemical Engineering, Fuzhou University, Fuzhou 350116, PR China

ARTICLE INFO

Article history:
Received 23 August 2013
Received in revised form
14 November 2013
Accepted 21 November 2013
Available online 24 December 2013

Keywords:
Alkaline media
Ethanol oxidation
Microwave-assisted
Pd-based catalysts
Palladium–tellurium

ABSTRACT

Carbon-supported palladium–tellurium binary nanocatalysts with different atomic ratios of Pd/Te ($PdTe_x$/C, x = 0.5, 1, 1.5 and 2) are prepared by a fast microwave polyol method. X-ray diffraction (XRD), transmission electron microscopy (TEM) and X-ray photoelectron spectroscopy (XPS) analysis reveal that the intermetallic phases of both PdTe and $PdTe_2$ are formed in the $PdTe_x$/C catalysts. The presence of tellurium effectively inhibits the agglomeration of Pd nanoparticles. All catalyst nanoparticles are uniformly dispersed on carbon support and the average particle size of $PdTe_{1.5}$/C catalyst is a bit smaller than that of Pd/C catalyst. The peak current density of ethanol oxidation on $PdTe_{1.5}$/C (190.3 mA cm^{-2}) is about 2.8 times higher than that on Pd/C (68.5 mA cm^{-2}) in cyclic voltammograms (CV). Moreover, the anti-poisoning ability and durability of this catalyst are also greatly improved. The Te-containing catalyst facilitates the formation of oxygenated species obviously and weakens the adsorption of CO-like species. The kinetics of ethanol oxidation reaction is notably enhanced on the $PdTe_{1.5}$/C catalyst.

Contents

1. Introduction

As a clean power source, direct alcohol fuel cells (DAFCs) have been studied extensively over the last few decades due to their high efficiency, high energy density and low pollutant emission [1–3]. Ethanol is considered one of the most promising renewable fuels, because it has high theoretical energy density (8.01 kWh kg^{-1}) and no toxicity, and can be easily produced in great quantities from fermentation of biomass [4]. Therefore, direct ethanol fuel cell (DEFC) has drawn enormous attention in recent years. However, the complete oxidation of ethanol to CO_2 involves 12 electrons transfer and the cleavage of C—C bond, which requires rather high activation energy [5]. Meanwhile, some poisonous intermediates generated from the dissociation of ethanol molecules can readily adsorb on catalyst surface and reduce the catalytic efficiency [6]. The kinetics of ethanol oxidation reaction (EOR) in acidic environment is still quite slow for a Pt-based catalyst, which is considered as the most suitable electrocatalyst [7]. Thus the commercialization of DEFC is still inhibited by the sluggish kinetics of EOR.

Recently, with the development of alkaline anion exchange membranes (AAEMs), the alkaline DEFC has attracted increasing interest [8]. The electrocatalytic activity of EOR on Pt-based catalysts in alkaline media has been proved to be significantly enhanced compared to that in acid media, indicating that the kinetics of EOR is faster in alkaline media [9,10]. In the previous researches, palladium has been certified as an effective electrocatalyst for ethanol electro-oxidation in alkaline media because of its high electrocatalytic activity and stability [11,12]. Moreover, Pd is cheaper and more abundant on the earth than Pt, and thus the catalyst cost can be conspicuously reduced [13]. Nevertheless, the activity of

* Corresponding author. Tel.: +86 591 8807 3608; fax: +86 591 8807 3608.
E-mail address: yguo@fzu.edu.cn (Y. Guo).

0926-3373/$ – see front matter © 2013 Elsevier B.V. All rights reserved.
http://dx.doi.org/10.1016/j.apcatb.2013.11.035

Pd catalyst for EOR in alkaline solution is still in need of enhancement to achieve the commercial application of DEFC. To improve the electrocatalytic activity of palladium, many composite catalysts including the Pd-based electrocatalysts with metal adatom modification, alloying and oxide doping have been developed successfully. Various bimetallic PdM (M = Ru, Sn, Au, Ag, Ni, Cu, Bi, etc.) catalysts have been investigated and present excellent electrocatalytic activity for EOR in alkaline media [14–21]. Besides, the addition of oxides such as ZrO_2, CeO_2, NiO, Co_3O_4, Mn_3O_4 and In_2O_3 can remarkably enhance the electrocatalytic activity and stability of Pd-based catalysts for EOR and lower the onset potential of ethanol oxidation [22,23].

Previous research results show that tellurium has a promotional effect on the electrooxidation of alcohols [24–26]. The incorporation of Te in the catalysts can enhance both the electrocatalytic activity and stability for alcohol oxidation. Huang et al. [24,25] prepared Pt_3Te_x/C by formic acid reduction and the microwave-polyol method, respectively, and found that the Pt_3Te/C catalyst exhibited higher catalytic activity for ethanol oxidation than commercial PtRu/C and Pt/C catalysts. The superior activity of Pt_3Te/C for ethanol oxidation is attributed to its high electrochemical active surface and/or the synergetic effect between Pt and Te. Guo et al. [26] reported that Pt–Te hybrid nanowire showed an enlarged electroactive surface area and higher electrocatalytic activity toward methanol oxidation reaction compared to commercial platinum black catalyst. To the best of authors' knowledge, however, ethanol electrooxidation on the PdTe bimetallic catalyst in alkaline media has not been investigated. In this work, the $PdTe_x$/C electrocatalysts with different atomic ratios of Pd/Te were prepared by the microwave polyol method. Their electrocatalytic activity toward EOR was investigated by different electrochemical techniques.

2. Experimental

2.1. Synthesis of $PdTe_x$/C catalysts

All reagents with analytical grade were used as received without any further purification. The active carbon black (Vulcan XC-72R), purchased from Cabot Corp., was pretreated with concentrated HNO_3 in a flask with a reflux set at 80 °C for 10 h. The mixture was diluted, filtered, washed with double-distilled water until neutral pH and dried at 80 °C overnight in a vacuum oven. The preparation procedures of the $PdTe_x$/C (x = 0, 0.5, 1, 1.5 and 2) catalysts were as follows: the H_2PdCl_4 aqueous solution was prepared by dissolving $PdCl_2$ in HCl aqueous solution. 15.6 mg of Vulcan XC-72R carbon was dispersed in 50 ml of ethylene glycol (EG) under ultrasonic stirring. The metal precursors of H_2PdCl_4 (37.8 mM) and Na_2TeO_4 (18.9 mM) with different Pd/Te atomic ratios were added to the suspension with constant stirring for 30 min. The pH value was adjusted to 10 by using KOH solution (0.4 M). The well-dispersed mixture was treated for 5 min in a flask with a reflux set under a microwave power of 800 W. Finally, the black product was filtered, washed and dried in a vacuum oven at 80 °C for 8 h. The total Pd loading of all catalysts in $PdTe_x$/C was maintained at 20 wt%.

2.2. Physical and electrochemical characterization

The XRD patterns of the prepared catalysts were obtained from a X-ray powder diffractometer (Philip X'Pert Pro MPP) using a Cu Kα radiation (λ = 1.5418 Å) at the scan rate of 2° min^{-1} with a step of 0.02°. The morphology and size distribution of the catalysts were examined by a transmission electron microscope (TEM, JEOL JEM-1010) with the accelerating voltage of 200 kV. The chemical valence state and the surface composition of the catalysts were carried out by the X-ray photoelectron spectroscopy (XPS, VG ESCALAB 250) using an Al Kα X-ray source of 1486.6 eV. The XPS spectra were recorded at the chamber pressure below 3×10^{-10} mbar and the C 1s electron binding energy was referenced at 284.6 eV.

Electrochemical measurements were carried out by a CHI 660C electrochemical working station (CH Instrument Inc.) in a typical three-electrode electrolytic cell. Glassy carbon electrode (GCE, 0.1256 cm^2) was used as the working electrode to support the catalysts. A piece of Pt foil and Hg/HgO/1 M KOH (MMO, 0.098 V vs. SHE [27]) were used as the counter and reference electrodes, respectively. The GCE was polished with Al_2O_3 paste, treated in an ultrasonic bath and then rinsed by double-distilled water and anhydrous ethanol in sequence. To prepare the working electrode, 5.0 mg as-prepared catalyst was dispersed in 1 ml solution of 985 μl of isopropyl alcohol and 15 μl of Nafion solution (15 wt%, DuPont) under ultrasonic stirring for 30 min. A 4 μl aliquot of the slurry was transferred onto the pre-polished GCE by using a micropipette and dried under an infrared lamp. The total Pd loading on the electrode kept 4 μg. Before measurements, the 1 M KOH or 1 M KOH + 1 M C_2H_5OH solution was first de-aerated with high purity N_2. All electrochemical measurements were performed at 30 ± 1 °C. Cyclic voltammograms (CV) were carried out between −0.95 and 0.5 V in 1 M KOH solution containing 1.0 M C_2H_5OH at a scan rate of 50 mV s^{-1}. Chronoamperometric measurements were conducted in 1 M KOH + 1 M C_2H_5OH solution at −0.3 V for 1800 s.

The CO stripping experiments were performed as follows: after de-aeration with N_2, CO was bubbled through the KOH solution in the electrolytic cell with the work electrode for 15 min. The residual CO in KOH solution was purged by high purity N_2 for 30 min prior to the stripping tests. Before all electrochemical measurements, stable CV curves were recorded after 20 cycles in the N_2-saturated blank KOH solution.

3. Results and discussion

The XRD patterns of Pd/C, Te/C and $PdTe_x$/C (x = 0.5, 1, 1.5 and 2) catalysts are shown in Fig. 1A. At about 25°, all diffractograms show that a broad peak refers to graphite (0 0 2) facet of carbon black. The XRD pattern of Te/C only displays two peaks at about 25° and 44°, which are indexed to carbon powder support. No obvious peaks of tellurium or its oxides in the XRD pattern of Te/C are observed, which implies that most tellurium or its oxide is in amorphous state. The three main diffraction peaks of Pd/C located at about 39.7°, 45.9° and 67.1° are attributed to the (1 1 1), (2 0 0) and (2 2 0) reflections of face centered cubic (*fcc*) Pd crystal (JCPDS Card No. 05-0681), respectively. For $PdTe_x$/C catalysts, all catalysts display the typical *fcc* crystalline structure of the metallic Pd, whereas $PdTe_x$/C catalysts present a shift of the diffraction peaks toward higher 2θ values with respect to Pd/C (Fig. 1B). It suggests the alloy formation between Pd and Te. As the Te amount increases in the $PdTe_x$/C catalysts, besides the Pd diffraction peaks, some slight peaks can also be found in $PdTe_2$/C catalyst, which are attributed to the formation of PdTe and $PdTe_2$ phases [27,28].

The average size of the catalytic nanoparticles (d) and the lattice parameter (a) can be estimated based on the broadening of the diffraction peaks of Pd(2 2 0) according to Scherrer formula [29] and Vegard's law [30], respectively.

$$d = \frac{0.9\lambda}{\beta \cos\theta} \quad (1)$$

$$a = \frac{\sqrt{2}\lambda}{\sin\theta} \quad (2)$$

where λ denotes the wavelength of X-ray (1.5418 Å), θ the angle of the Pd(2 2 0) peak, and β its half-peak width. The average particle size and the lattice parameter of the catalysts are shown in Table 1. It indicates that the crystallite size and the lattice parameter of the

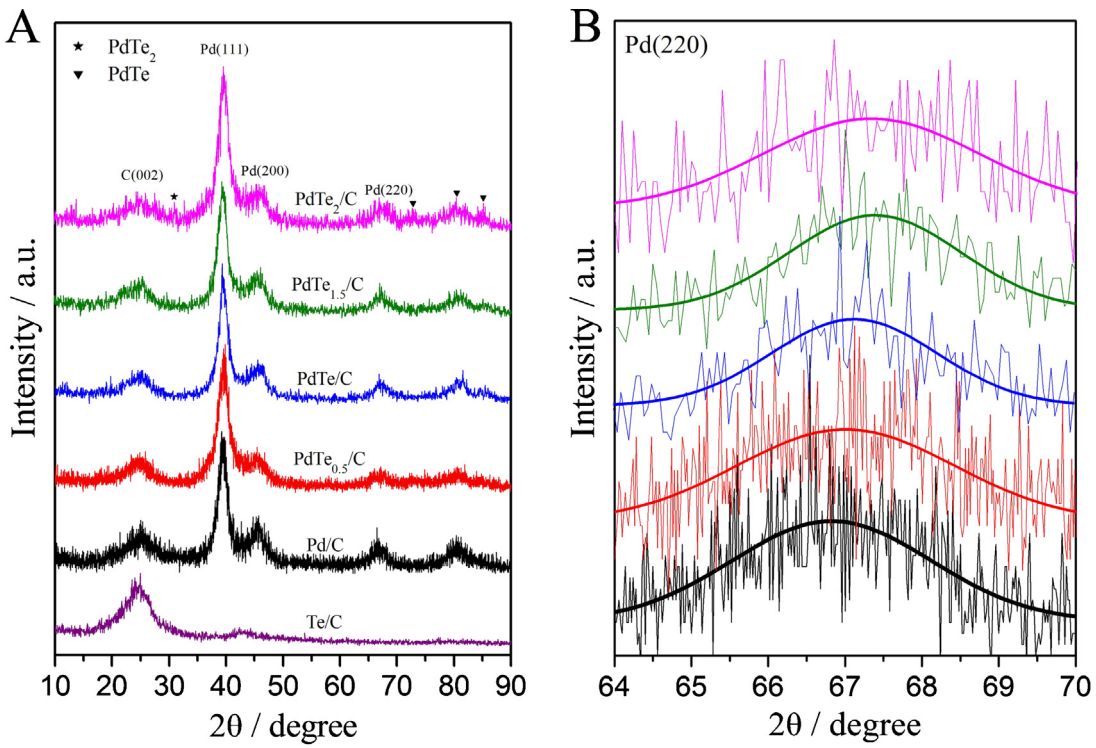

Fig. 1. (A) XRD patterns and (B) the magnified Pd(2 2 0) peaks of Pd/C and $PdTe_x$/C catalysts with different atomic ratios of Pd/Te.

catalytic nanoparticles have a slight reduction after combining Te with Pd catalyst.

TEM images were employed to observe the morphology and the particle-size distribution of Pd/C and $PdTe_{1.5}$/C catalysts. As shown in Fig. 2A and 2B, the catalyst nanoparticles are highly dispersed on the carbon support in both catalysts and a little agglomeration occurs in Pd/C catalyst. It seems that the microwave-assisted method easily results in the agglomeration of Pd nanoparticles in the synthesis of Pd/C catalyst, which was also reported in Refs. [20,31,32]. The rapid growth of Pd nuclei during microwave heating tends to induce Pd aggregation [32]. However, the metal nanoparticles in $PdTe_{1.5}$/C catalyst have a more uniform dispersion on the carbon support compared to those in the Pd/C catalyst. The probable explanation is that the presence of Te around the Pd nuclei decreases the affinity among Pd atoms. The insets in Fig. 2A and B show the high-resolution TEM (HRTEM) images of the nanoparticles in the Pd/C and $PdTe_{1.5}$/C catalysts, respectively. There are two typical lattice distances with approximately 2.27 and 1.88 Å on the Pd/C catalyst, which are indexed to the Pd(1 1 1) and Pd(2 0 0) planes, respectively. For the $PdTe_{1.5}$/C catalyst besides the planes of Pd metal, four groups of lattice stripes with interplanar spacing of 2.01, 2.56, 2.07 and 3.02 Å are also found, which are corresponding to the $PdTe_2$ (1 1 0), $PdTe_2$ (0 0 2), PdTe (1 1 0) and PdTe (1 0 1) planes (JCPDS card No. 65-1901 and 65-9516). It is confirmed that the PdTe and $PdTe_2$ phases were formed in the $PdTe_{1.5}$/C catalyst. Besides, the Pd separate phase appears in the outer layers of some nanoparticles, indicating that only a partial of Pd presents intermetallic phase. The particle size distribution of the nanoparticles in the Pd/C and $PdTe_{1.5}$/C catalysts (Fig. 2C and D) was determined by the statistic analysis of more than 500 particles in arbitrarily selected area of the corresponding TEM images. The average particle size of Pd/C and $PdTe_{1.5}$/C catalysts are 4.4 and 4.3 nm, respectively. Therefore, the presence of Te and PdTe alloying reduce the affinity among Pd atoms and impede the growth of Pd nanoparticles greatly so that the $PdTe_{1.5}$/C catalyst has smaller particle size compared to the Pd/C catalyst, which is in good agreement with the XRD analysis.

The XPS test was used to determine the surface oxidation states of the elements in Pd/C and $PdTe_{1.5}$/C catalysts. As can be seen in Fig. 3A, the Pd/C catalyst displays two asymmetrical peaks with high energy band (Pd $3d_{3/2}$) at 340.95 eV and low energy band (Pd $3d_{5/2}$) at 335.65 eV in Pd 3d signal region, while the two peaks for the Pd $Te_{1.5}$/C catalyst are located at 341.05 and 335.85 eV. The positive shift of Pd binding energy for Pd $Te_{1.5}$/C compared to Pd/C indicates the electronic interaction between palladium and tellurium, such as a charge transfer process from Pd to Te [25]. It indicates that the Pd d-band center shifts down when Pd is alloyed with Te according to the d-band theory [33]. The downshift of Pd d-band results in the decrease of the amount of adsorbates (such as CO-like species) on Pd surface [34,35]. The Pd 3d signal of Pd/C is fitted to three doublets, which can be assigned to metallic Pd(0), PdO_{ads} and PdO, respectively [20]. The binding energy of each peak in Pd

Table 1
Results of XRD and CV data of Pd/C and $PdTe_x$/C catalysts.

Samples	Average particle size (nm)	Lattice parameters (Å)	EASA[a] ($m^2\ g^{-1}$)	Onset potentials (V)	Peak current density ($mA\ cm^{-2}$)
Pd/C	4.0	3.967	31.6	−0.48	68.5
$PdTe_{0.5}$/C	3.8	3.947	39.4	−0.52	92.5
PdTe/C	3.8	3.936	32.7	−0.55	126.1
$PdTe_{1.5}$/C	3.7	3.935	42.3	−0.61	190.3
$PdTe_2$/C	3.7	3.926	48.8	−0.50	76.9

[a] The electrochemical active surface area.

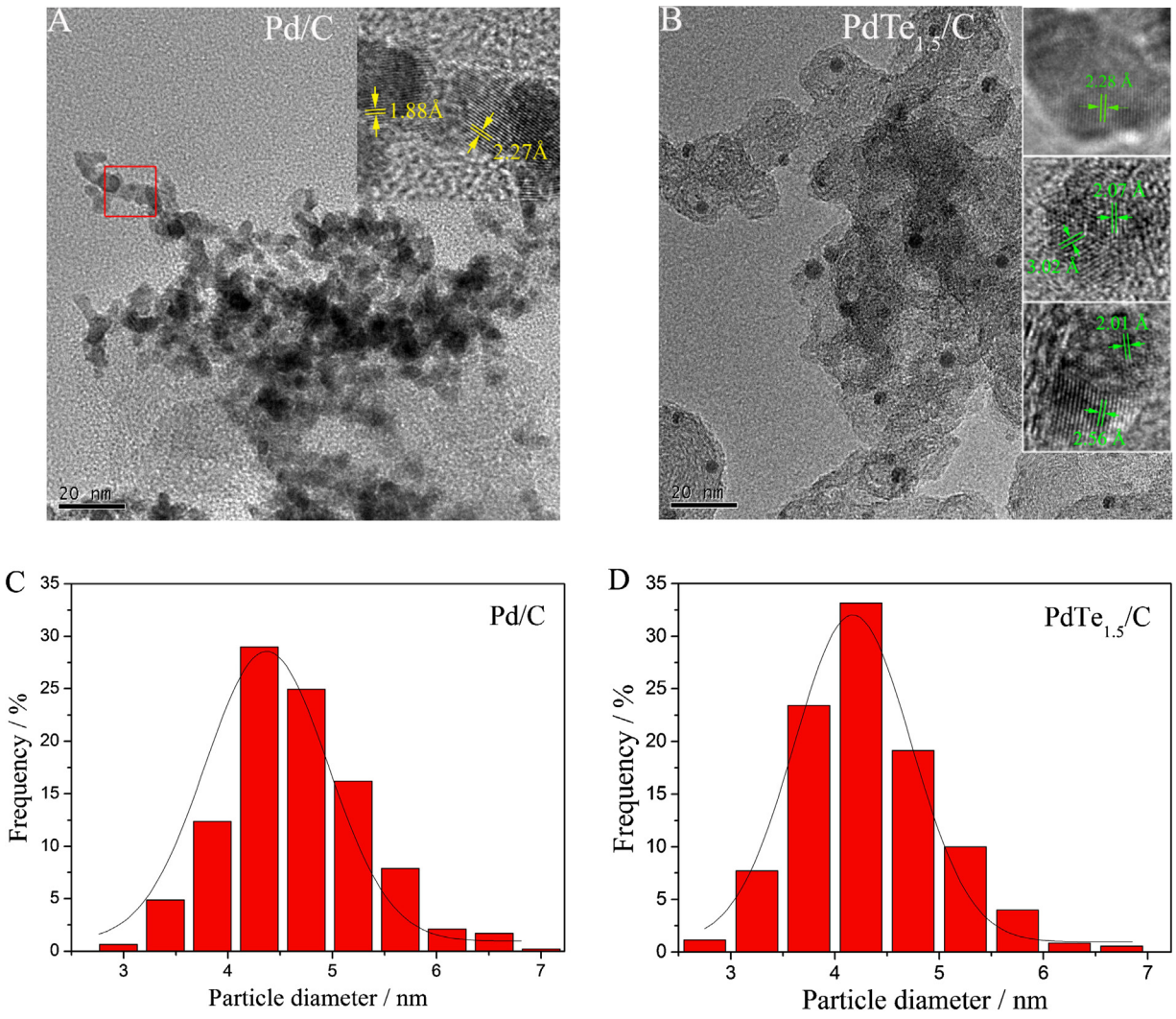

Fig. 2. TEM images and particle size distribution histograms of (A and C) Pd/C and (B and D) $PdTe_{1.5}$/C.

$3d_{5/2}$ region is 5.3 eV lower than that of the corresponding ones in Pd $3d_{3/2}$ region. For the $PdTe_{1.5}$/C catalyst, the Pd 3d signal consists of two doublets indexed to Pd and PdO_{ads}. The relative content of metallic Pd calculated from the relative peak intensity is 50.9% in Pd/C catalyst and 83.7% in $PdTe_{1.5}$/C catalyst, respectively. This suggests that Te addition reduces the formation of Pd oxides. For the Te region in Fig. 3B, the doublet consisting of a high energy band at 584.4 (Te $3d_{3/2}$) and a low energy band at 573.9 eV (Te $3d_{5/2}$) corresponds to elemental state Te(0), and the other doublet at 586.1 and 575.6 eV corresponds to TeO_2 [25]. The binding energy of high energy band (Te $3d_{3/2}$) is 10.5 eV higher than that of the low energy band (Te $3d_{5/2}$). The relative content of elemental state Te(0) and TeO_2 in the $PdTe_{1.5}$/C catalyst is 86.7% and 13.3%, respectively.

The CV curves of Pd/C and $PdTe_x$/C catalysts in 1 M KOH solution are shown in Fig. 4. It is found that an obvious peak is located at about −0.7 V on Pd/C catalyst in the positive-going sweep, which is related to the oxidation of adsorbed hydrogen on the palladium surface. In the negative-going sweep, the peak at about −0.28 V can be ascribed to the reduction of PdO into Pd(0) [36]. The peak at about −0.55 V is assigned to the adsorption of OH^- on the palladium surface [36,37]. It can be observed that the peak currents of OH^- adsorption and hydrogen desorption gradually decrease with the increase of Te amount in $PdTe_x$/C catalysts. Besides, an obvious oxidation peak appears at around 0.05 V on $PdTe_x$/C catalysts and can be attributed to the formation of Te oxides on surface [19,20,36]. In the negative-going sweep, the reduction peak at about −0.28 V becomes higher and higher with the increase of Te amount. Because the Pd loading is fixed, this reduction peak is ascribed to the simultaneous reduction of PdO and TeO_2. Besides the property of the catalyst, the geometrical area also influences the activity of a catalyst. The electrochemical active surface area (EASA) has also been measured by integrating the charge in the reduction of palladium oxide [38]. The EASA of Pd can be evaluated according to the following equation:

$$EASA = \frac{Q}{SI} \tag{3}$$

where Q denotes the Coulombic charge of PdO reduction, I the loadings of Pd catalyst, and S the conversion factor with the value of 405 μC cm^{-2} assumed for the reduction of PdO monolayer [39]. The EASA values calculated from PdO reduction are shown in Table 1. The high EASA is beneficial for the electrocatalytic activity of the catalyst.

The stable open circuit potential (OCP) was used to study the mixed potential of redox reactions on electrode surface. The evolution of OCP on Pd/C and $PdTe_x$/C catalysts was obtained after 10 CV cycles in 1 M KOH, as displayed in Fig. 5. It is found that the OCP ascends quickly at the initial stage and then tends to be stable. With the increase of Te amount in $PdTe_x$/C catalysts, the OCP rising become increasingly fast. This is attributed to the mixed

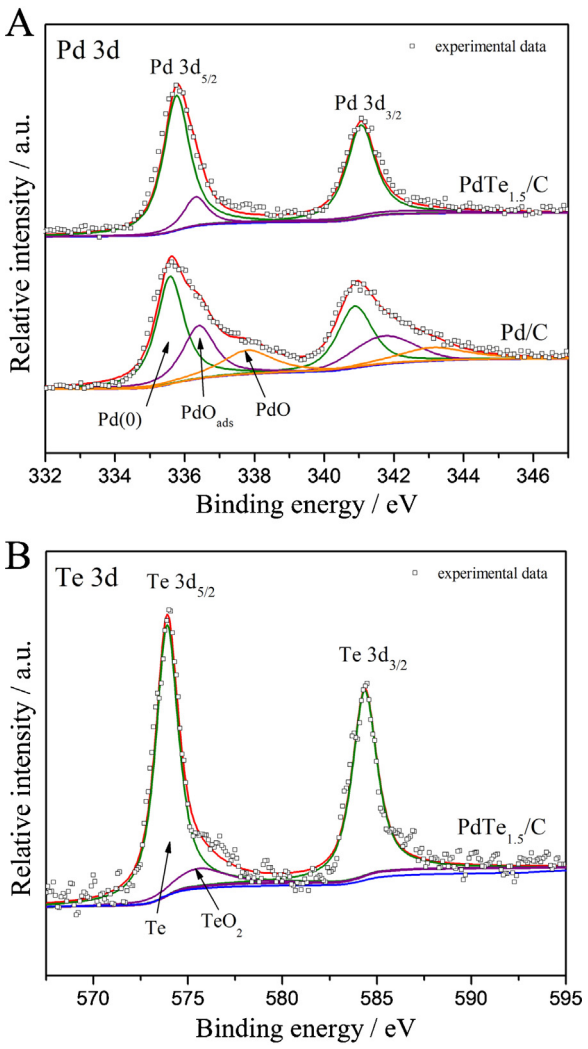

Fig. 3. XPS spectra of (A) Pd/C and $PdTe_{1.5}$/C in Pd 3d region and (B) $PdTe_{1.5}$/C in Te 3d region.

potential established by the $PdTe_x$/C catalyst surface in the presence of oxygen-containing species [20,40,41]. According to the oxidation and reduction peak potential of oxygen-containing species in Fig. 4, their equilibrium potential is approximately equal to

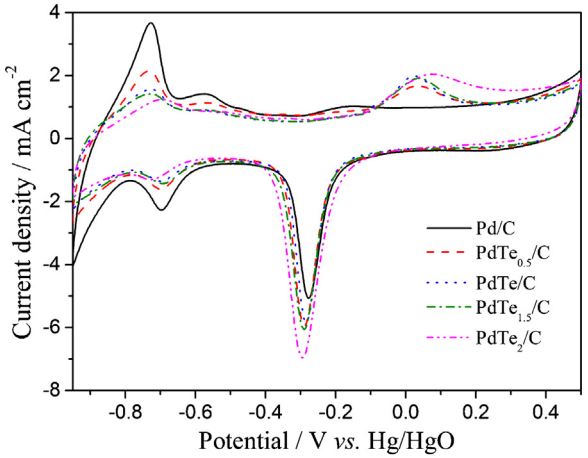

Fig. 4. Cyclic voltammograms of Pd/C and $PdTe_x$/C catalysts with different atomic ratios in 1 M KOH solution. Scan rate: 50 mV s^{-1}.

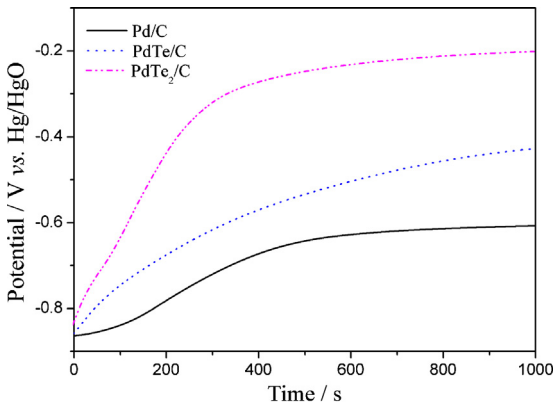

Fig. 5. Evolution of the open circuit potentials (OCP) on Pd/C and $PdTe_x$/C catalysts with different atomic ratios in 1 M KOH solution.

−0.1 V. The more the amount of oxygen-containing species on the electrode surface is, the closer to their equilibrium potentials the stable value of the mixed potential on open circuit is. Therefore, the presence of Te in $PdTe_x$/C catalysts promotes greatly the formation of more oxygen-containing species on the catalyst surface. It is well known that the oxygenated species are significant for ethanol oxidation because they can increase the concentration of hydroxyl on the catalyst surface, thereby promoting the oxidation of poisoning intermediates via a bifunctional mechanism [42,43].

The electrocatalytic activity of Pd/C and $PdTe_x$/C catalysts with different Pd/Te atomic ratios for EOR was examined by CV in 1 M KOH + 1 M C_2H_5OH solution. The currents are normalized with respect to the catalyst activity area. Fig. 6 only shows the positive-going potential sweep part of CV curves for clear observation. It is interesting to note that the addition of Te greatly enhances the electrocatalytic activity of Pd catalyst for ethanol oxidation in alkaline medium. The maximum peak current density of ethanol oxidation appears on the $PdTe_{1.5}$/C catalyst (190.3 mA cm^{-2}), which is about 2.8 times higher than that on the Pd/C catalyst (68.5 mA cm^{-2}). Furthermore, the onset potential of ethanol oxidation on the $PdTe_{1.5}$/C catalyst shifts more negatively than those on other samples. The peak current densities of ethanol oxidation and their onset potentials on these catalysts are shown in Table 1. Therefore, the $PdTe_{1.5}$/C catalyst exhibits the best electrocatalytic activity for ethanol oxidation among these catalysts. This enhancement can be explained by the electronic effect and the bifunctional mechanism [24], which will be discussed in more details in the section below. However, further increase of Te composition on the $PdTe_2$/C catalyst results in a reduction of peak current density, which is mainly

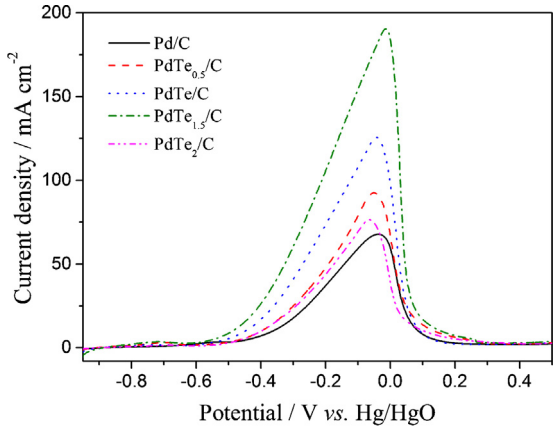

Fig. 6. Positive-going potential sweep curves of Pd/C and $PdTe_x$/C catalysts with different atomic ratios in 1 M KOH + 1 M C_2H_5OH solution.

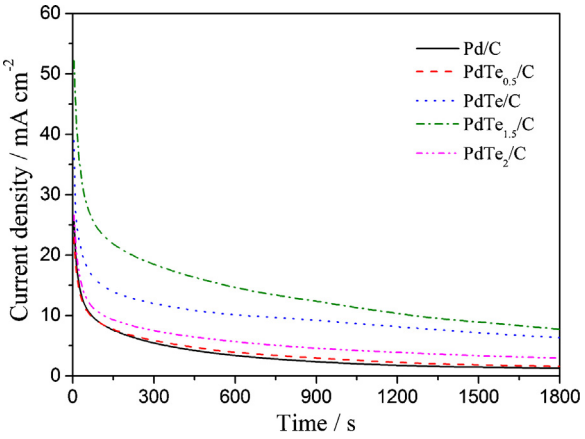

Fig. 7. Current–time curves of Pd/C and $PdTe_x$/C catalysts with different atomic ratios at −0.3 V in 1 M KOH + 1 M C_2H_5OH solution.

due to the poor electronic conductivity of the catalyst or excessive coverage of Pd active sites for ethanol oxidation [20,40].

The electrocatalytic stability of the as-prepared catalysts for ethanol oxidation was studied by the chronoamperometry in 1 M KOH + 1 M C_2H_5OH solution at −0.3 V, as shown in Fig. 7. The current densities on all catalysts decline quickly at the initial stage, then fall slowly and approach a relative stable state. This phenomenon can be explained as follows: the poisonous intermediates generated from the continuous EOR gradually accumulate on the catalyst surface and hinder the further oxidation of ethanol; when it comes to the relative stable state, the kinetics of the adsorbed intermediates removal almost keeps pace with that of ethanol oxidation [44]. It is found that the current densities of $PdTe_x$/C catalysts are higher than that of Pd/C catalyst, indicating that the Te addition enhances the durability and poisoning-tolerance of Pd catalyst. The stable current densities on these catalysts are in the following order: $PdTe_{1.5}$/C > PdTe/C > $PdTe_{0.5}$/C > $PdTe_2$/C > Pd/C, in accordance with the results obtained in CVs of Fig. 6. The steady current density on $PdTe_{1.5}$/C (7.8 mA cm^{-2}) keeps the highest among these catalysts, which is 6.5 times higher than the value on Pd/C (1.2 mA cm^{-2}). Therefore, the $PdTe_{1.5}$/C catalyst has the best catalytic stability.

Linear current sweep is a valid approach to investigate the anti-poisoning ability of as-prepared catalysts [45]. The current sweep experiments were performed at the scan rate of 0.16 mA cm^{-2} s^{-1} in 1 M KOH + 1 M C_2H_5OH solution, which are shown in Fig. 8. As the polarization current increases, various electrochemical polarizations increase simultaneously. At the same time, the accumulation of poisonous intermediates also occurs on the catalyst surface. In

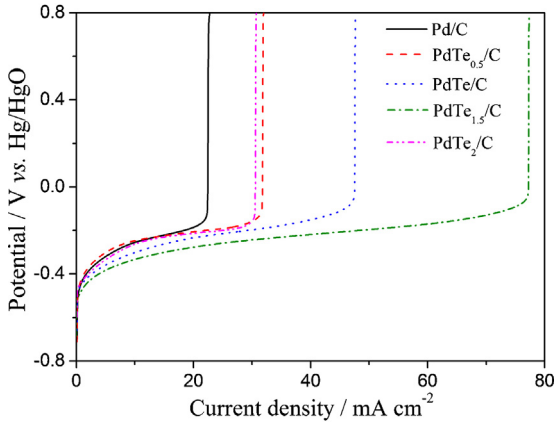

Fig. 8. Linear current sweep curves of Pd/C and $PdTe_x$/C catalysts with different atomic ratios at the scan rate of 0.16 mA cm^{-2} s^{-1} in 1 M KOH + 1 M C_2H_5OH solution.

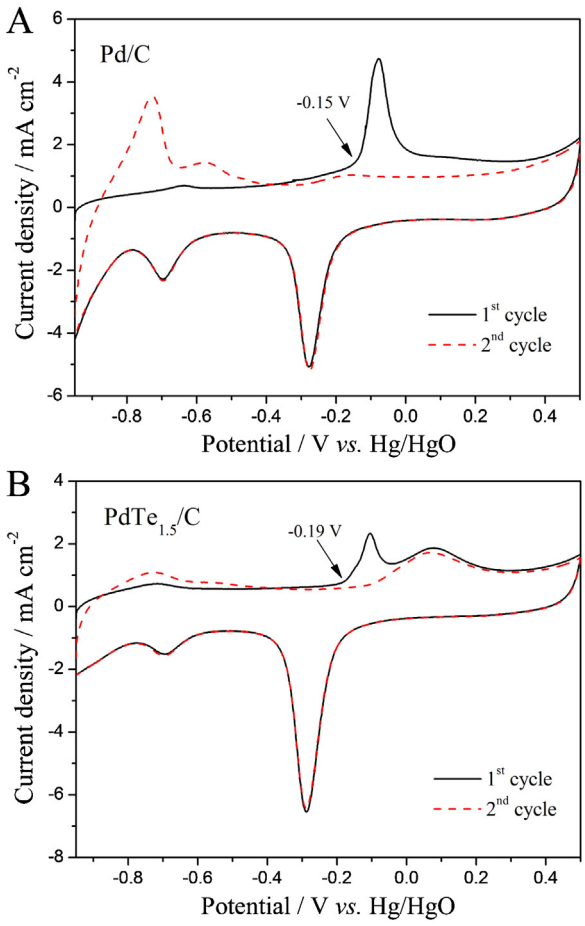

Fig. 9. CO stripping curves on (A) Pd/C and (B) $PdTe_{1.5}$/C in 1 M KOH solution.

order to satisfy the applied current, sufficient oxygenated species should be generated by raising polarization potential to oxidize poisonous intermediate species [20,40]. When these intermediate species accumulate and cover the active sites completely, the catalyst surface poisons and the potential begins to leap to a very high value for oxygen evolution instead of the ethanol oxidation [46]. Thus the catalyst with lower polarization potential and higher current density at skipping potential has better poisoning-tolerance. Among as-prepared catalysts, the $PdTe_{1.5}$/C catalyst exhibits the lowest polarization potential and highest current density at the point of steep hop in potential, confirming that the $PdTe_{1.5}$/C catalyst has best poisoning tolerance towards CO-like species.

CO stripping test was employed to evaluate the capability of the catalyst in removal of adsorbed CO-like species. Fig. 9 displays the CO-stripping curves of Pd/C and $PdTe_{1.5}$/C catalysts in 1 M KOH solution. As shown in Fig. 9, the absence of the hydrogen desorption peaks in the 1st cycle indicates the saturated adsorption of CO on the catalyst surface. The onset potential of CO oxidation on $PdTe_{1.5}$/C is more negative than that on Pd/C. Besides, the peak potential of CO oxidation on $PdTe_{1.5}$/C catalyst shifts negatively ca. 30 mV compared with Pd/C catalyst. These results indicate that the incorporation of Te facilitates CO oxidation from the catalyst surface. Moreover, the CO stripping peak current density on $PdTe_{1.5}$/C catalyst conspicuously decreases compared to Pd/C catalyst. The explanation is as follows: (i) Alloying between Pd and Te leads to the decrease of Pd active sites on $PdTe_{1.5}$/C binary catalyst surface and (ii) the electronic effect of Te on Pd suppresses the CO adsorption on Pd surface as proposed by the d-band theory [34,35,47]. The second oxidation peak at about 0.1 V on $PdTe_{1.5}$/C catalyst in the

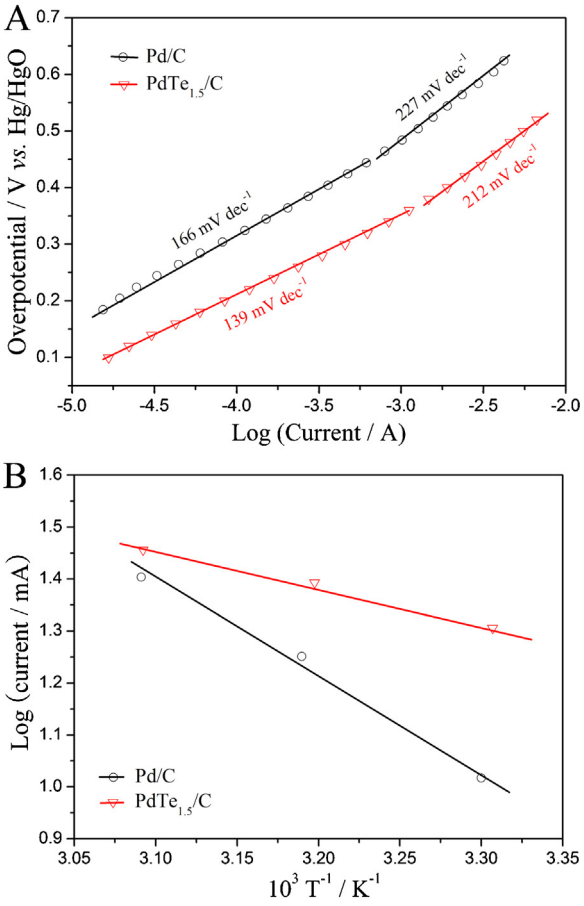

Fig. 10. (A) Tafel plots and (B) Arrhenius plots on Pd/C and $PdTe_{1.5}$/C catalysts in 1 M KOH + 1 M C_2H_5OH solution.

CO stripping curve is ascribed to the formation of surface oxygen species [20,47].

It is well known that the effect of the promoter in binary catalyst is explained mainly in terms of the electronic effect and/or the bifunctional mechanism. The XPS results reveal that electronic interaction between Pd and Te exists in $PdTe_{1.5}$/C catalyst. The addition of Te causes the Pd d-band centre to shift down, which results in weakening adsorption of CO-like species in Pd surface as discussed in CO stripping [33–35]. On the other hand, the onset potentials of EOR and CO oxidation on $PdTe_{1.5}$/C catalyst are more negative compared to those on Pd/C catalyst, implying that $PdTe_{1.5}$/C can facilitate the removal of adsorbed intermediates on catalyst surface. The OCP curves show that the oxygen-containing species easily form on $PdTe_x$/C catalysts, which can promote the oxidation of poisoning intermediates via the bifunctional mechanism [42,43]. From the discussion above, the enhanced activity and stability of $PdTe_{1.5}$/C catalyst are attributed to the electronic effect and the bifunctional mechanism.

Fig. 10 presents Tafel plots and Arrhenius plots for Pd/C and $PdTe_{1.5}$/C catalysts to further study the kinetics of ethanol oxidation. The Tafel plots of these two catalysts were obtained in 1 M KOH + 1 M C_2H_5OH solution. As shown in Fig. 10A, the curves of both catalysts show two linear regions, indicating the different EOR mechanisms caused by the adsorption of hydroxyl in low potential region and by the formation of the oxide layer on the Pd surface in high potential region [37]. The Tafel slope values in these two regions are 139 and 212 mV dec^{-1} for $PdTe_{1.5}$/C catalyst, 166 and 227 mV dec^{-1} for Pd/C catalyst, respectively. The exchange current density can be evaluated by extrapolating the Tafel line in the low potential region. The exchange current density (normalized to geometrical area of the electrode) on the $PdTe_{1.5}$/C (2.53×10^{-5} A cm^{-2}) is higher than that on Pd/C (9.6×10^{-6} A cm^{-2}), indicating that the $PdTe_{1.5}$/C has a faster charge transfer kinetics and higher catalytic activity for ethanol oxidation in alkaline medium [48]. Fig. 10B shows the Arrhenius plots of EOR on the Pd/C and $PdTe_{1.5}$/C catalysts based on the currents at −0.1 V and at different temperatures. The apparent activation energy calculated according to Arrhenius equation [49] are 33.67 and 15.12 kJ mol^{-1} on Pd/C and $PdTe_{1.5}$/C catalysts, respectively. The smaller apparent activation energy further indicates the faster charge-transfer process and higher intrinsic activity for EOR on the $PdTe_{1.5}$/C catalyst [16,50].

4. Conclusions

Novel $PdTe_x$/C catalyst has been prepared by a fast microwave polyol method. The physical characterizations reveal the uniform dispersion of $PdTe_x$/C catalyst and the formation of PdTe and $PdTe_2$ alloys on the carbon support. The OCP of Te-containing catalysts shift positively with the increase of Te amount, indicating that the Te addition promotes adsorption of oxygenated species on catalyst surface. These oxygenated species can greatly facilitate the oxidation of poisoning intermediates at low potential and then release free Pd active sites for further adsorption and electro-oxidation of ethanol. Thus, the onset potentials of ethanol oxidation on $PdTe_x$/C catalysts are more negative than that on Pd/C catalyst. The peak current densities are in the following order: $PdTe_{1.5}$/C > PdTe/C > $PdTe_{0.5}$/C > $PdTe_2$/C > Pd/C. And they are 190.3 and 68.5 mA cm^{-2} on $PdTe_{1.5}$/C and Pd/C catalysts, respectively. The results of CO stripping test confirm that the addition of Te can weaken the adsorption of CO-like species and facilitate the oxidative removal of CO-like species on catalyst surface. The appropriate amount of Te greatly promotes the kinetics of ethanol oxidation on Pd catalyst. The enhanced activity and stability of $PdTe_x$/C catalysts for EOR are attributed to the electronic effect and the bifunctional mechanism.

Acknowledgments

The authors are grateful to the NSFC (No. 51072037) in China and Natural Science Foundation of Fujian Province (No. 2013J01039) for financial support of this work.

References

[1] W. Zhou, Z. Zhou, S. Song, W. Li, G. Sun, P. Tsiakaras, Q. Xin, Appl. Catal. B: Environ. 46 (2003) 273.
[2] C. Lamy, A. Lima, V. LeRhun, F. Delime, C. Coutanceau, J.M. Léger, J. Power Sources 105 (2002) 283.
[3] G. Girishkumar, T.D. Hall, K. Vinodgopal, P.V. Kamat, J. Phys. Chem. B 110 (2006) 107–114.
[4] E.V. Spinacé, A.O. Neto, M. Linardi, J. Power Sources 124 (2003) 426.
[5] J.C.M. Silva, R.F.B. De Souza, L.S. Parreira, E. Teixeira Neto, M.L. Calegaro, M.C. Santos, Appl. Catal. B: Environ. 99 (2010) 265.
[6] R.F.B. De Souza, A.E.A. Flausino, D.C. Rascio, R.T.S. Oliveira, E. Teixeira Neto, M.L. Calegaro, M.C. Santos, Appl. Catal. B: Environ. 91 (2009) 516.
[7] E. Antolini, J. Power Sources 170 (2007) 1.
[8] E. Antolini, E.R. Gonzalez, J. Power Sources 195 (2010) 3431.
[9] S.C.S. Lai, M.T.M. Koper, Phys. Chem. Chem. Phys. 11 (2009) 10446.
[10] L. Jiang, A. Hsu, D. Chu, R. Chen, Int. J. Hydrogen Energy 35 (2010) 365.
[11] S. Shen, T. Zhao, J. Xu, Y. Li, J. Power Sources 195 (2010) 1001.
[12] C. Bianchini, P. Shen, Chem. Rev. 109 (2009) 4183–4206.
[13] H. Liu, W. Li, A. Manthiram, Appl. Catal. B: Environ. 90 (2009) 184.
[14] R.M. Modibedi, T. Masombuka, M.K. Mathe, Int. J. Hydrogen Energy 36 (2011) 4664.
[15] J. Xu, T. Zhao, S. Shen, Y. Li, Int. J. Hydrogen Energy 35 (2010) 6490.
[16] S.T. Nguyen, H.M. Law, H.T. Nguyen, N. Kristian, S. Wang, S.H. Chan, X. Wang, Appl. Catal. B: Environ. 91 (2009) 507.
[17] T. Maiyalagan, K. Scott, J. Power Sources 195 (2010) 5246.
[18] W. Kang, Y. Wei, C. Liu, K. Wang, Electrochem. Commun. 13 (2011) 162.
[19] A.O. Neto, M.M. Tusi, N.S.O. Polanco, S.G. da Silva, M.C. dos Santos, E.V. Spinacé, Int. J. Hydrogen Energy 36 (2011) 10522.

[20] J. Cai, Y. Huang, Y. Guo, Electrochim. Acta 99 (2013) 22.
[21] S.T. Nguyen, Y. Yang, X. Wang, Appl. Catal. B: Environ. 113–114 (2012) 261.
[22] C. Xu, Z. Tian, P.K. Shen, S.P. Jiang, Electrochim. Acta 53 (2008) 2610.
[23] D. Chu, J. Wang, S. Wang, L. Zha, J. He, Y. Hou, Y. Yan, H. Lin, Z. Tian, Catal. Commun. 10 (2009) 955.
[24] M. Huang, F. Wang, L. Li, Y. Guo, J. Power Sources 178 (2008) 48.
[25] M. Huang, L. Li, Y. Guo, Electrochim. Acta 54 (2009) 3303.
[26] S. Guo, S. Dong, E. Wang, J. Phys. Chem. C 114 (2010) 4797.
[27] I.A. Witońska, M.J. Walock, P. Dziugan, S. Karski, A.V. Stanishevsky, Appl. Surf. Sci. 273 (2013) 330.
[28] I. Witońska, M. Frajtak, S. Karski, Appl. Catal. A: Gen. 401 (2011) 73.
[29] J.M. Sieben, M.M.E. Duart, Int. J. Hydrogen Energy 36 (2011) 3313.
[30] J. Lobato, P. Cañizares, D. Ubeda, F.J. Pinar, M.A. Rodrigo, Appl. Catal. B: Environ. 106 (2011) 174.
[31] T. Ramulifho, K.I. Ozoemena, R.M. Modibedi, C.J. Jafta, M.K. Mathe, Electrochim. Acta 59 (2012) 310.
[32] C. Hsieh, Y. Liu, Y. Cheng, W. Chen, Electrochim. Acta 56 (2011) 6336.
[33] K. Wu, X. Mao, Y. Liang, Y. Chen, Y. Tang, Y. Zhou, J. Lin, C. Ma, T. Lu, J. Power Sources 219 (2012) 258.
[34] Jeff Greeley, J.K. Nørskov, Surf. Sci. 592 (2005) 104.
[35] U.B. Demirci, J. Power Sources 173 (2007) 11.
[36] Y. Wei, C. Liu, W. Kang, C. Lai, L. Tsai, K. Wang, J. Electroanal. Chem. 660 (2011) 64.
[37] Z. Liang, T. Zhao, J. Xu, L. Zhu, Electrochim. Acta 54 (2009) 2203.
[38] L. Jiang, A. Hsu, D. Chu, R. Chen, J. Electrochem. Soc. 156 (2009) B643.
[39] T. Chierchie, C. Mayer, W.J. Lorenz, J. Electroanal. Chem. Interfacial Electrochem. 135 (1982) 211.
[40] Y. Huang, J. Cai, Y. Guo, Appl. Catal. B: Environ. 129 (2013) 549.
[41] B. Peng, J. Wang, H. Zhang, Y. Lin, W. Cai, Electrochem. Commun. 11 (2009) 831.
[42] Y. Ye, H.S. Kim, P.K. Babu, P. Waszczuk, A. Wieckowski, E. Oldfield, J. Am. Chem. Soc. 124 (2002) 468.
[43] M. Chatterjee, A. Chatterjee, S. Ghosh, I. Basumallick, Electrochim. Acta 54 (2009) 7299.
[44] X. Zhang, H. Zhu, Z. Guo, Y. Wei, J. Power Sources 196 (2011) 3048.
[45] J. Lee, C. Eickes, M. Eiswirth, Electrochim. Acta 47 (2002) 2297.
[46] F. Hu, F. Ding, S. Song, P. Shen, J. Power Sources 163 (2006) 415.
[47] Q. Jiang, L. Jiang, J. Qi, S. Wang, G. Sun, Electrochim. Acta 56 (2011) 6431.
[48] L. Feng, J. Yang, Y. Hu, J. Zhu, C. Liu, W. Xing, Int. J. Hydrogen Energy 37 (2012) 4812.
[49] J.L. Cohen, D.J. Volpe, H.D. Abruna, Phys. Chem. Chem. Phys. 9 (2007) 49.
[50] Y. Wang, T.S. Nguyen, X. Liu, X. Wang, J. Power Sources 195 (2010) 2619.